Compressive strain induced enhancement of exchange interaction and short-range magnetic order in Sr_{2}IrO_{4} investigated by Raman spectroscopy

A. Seo, P. P. Stavropoulos, H.-H. Kim, K. Fürsich, M. Souri, J. G. Connell, H. Gretarsson, M. Minola, H. Y. Kee, and B. Keimer

Phys. Rev. B **100**, 165106 — Published 4 October 2019

DOI: 10.1103/PhysRevB.100.165106

Compressive-strain induced enhancement of exchange interactions and short-range magnetic order in Sr_2IrO_4 investigated by Raman spectroscopy

A. Seo,[1,2] P. P. Stavropoulos,[3] H.-H. Kim,[2] K. Fürsich,[2] M. Souri,[1] J. G. Connell,[1] H. Gretarsson,[2] M. Minola,[2] H. Y. Kee,[3] and B. Keimer[2]

[1.] *Department of Physics and Astronomy, University of Kentucky, 500 Rose St., Lexington, Kentucky 40506, USA*

[2.] *Max-Planck-Institut für Festkörperforschung, Heisenbergstraße 1, D-70569 Stuttgart, Germany*

[3.] *Department of Physics, University of Toronto, 60 St. George St., Toronto, Ontario, Canada M5S 1A7*

Abstract

We have carried out Raman spectroscopy experiments to investigate two-magnon excitations in epitaxial thin films of the quasi-two-dimensional antiferromagnetic Mott insulator Sr_2IrO_4 under in-plane misfit strain. With in-plane biaxial compression, the energy of the two-magnon peak increases, and the peak remains observable over a wider temperature range above the Néel temperature, indicating a strain-induced enhancement of the superexchange interactions between $J_{\mathrm{eff}} = 1/2$ pseudospins. From density functional theory calculations, we have found an increase of the nearest-neighbor hopping parameter and exchange interaction with increasing biaxial compressive strain, in agreement with the experimental observations. Our experimental and theoretical results provide perspectives for systematic, theory-guided strain control of the primary exchange interactions in 5*d* transition metal oxides.

I. INTRODUCTION

The coupling between different interactions with similar energy scales leads to new ground states in solids. Among many examples, the interplay between the relativistic spin-orbit interaction (λ) and the on-site Coulomb interaction (U) in materials with strongly correlated electrons has attracted great attention. Depending on their energy scales, the confluence of these two interactions is expected to result in novel phases such as Weyl semimetals, axion insulators, topological Mott insulators, etc. [1]. Indeed, spin-orbit coupled Mott insulators with $J_{\mathrm{eff}} = 1/2$ pseudospins have been discovered in 5*d* systems such as the layered iridates Sr_2IrO_4 [2] and Na_2IrO_3 [3] where the energy scales of λ and U are comparable.

The $J_{\mathrm{eff}} = 1/2$ pseudospins and their exchange interactions have been considered as analogs of spin $S = 1/2$ states. The mapping of the $J_{\mathrm{eff}} = 1/2$ pseudospin into $S = 1/2$ on a square lattice makes the quasi-two-dimensional (quasi-2D) magnetism in Sr_2IrO_4 closely comparable to La_2CuO_4, which is a parent compound of the high-temperature superconducting cuprates. Recent theoretical and experimental studies have focused on the similarities of both systems [4-7]. However, while the $S = 1/2$ electrons of the Cu^{2+} ions reside in non-degenerate e_g orbitals and therefore exhibit weak coupling with the lattice, the $J_{\mathrm{eff}} = 1/2$ pseudospin wave function of Ir^{4+} ions in iridates is an entangled state of both spin-up and spin-down states and all t_{2g} orbitals [2,8]. Therefore, multiple *d*-orbitals must be considered for a realistic description of the layered iridates, in analogy to multi-orbital systems such as the manganates and contrast to the orbitally non-degenerate cuprates. Note that the multi-spin/orbital characteristic can provide an intriguing scheme of enabling the manipulation of fundamental interactions via external parameters. For example, one could tune the magnetic exchange interaction of the layered iridates by applying external strain to its lattice. In fact, the exchange interaction plays an important role not only in magnetism but also in novel electronic properties. For instance, short-range antiferromagnetic correlations and spin fluctuations, which are governed primarily by nearest-neighbor superexchange interactions, are thought to be key to understanding the pairing mechanisms of unconventional superconductors such as the cuprates, Fe-pnictides, chalcogenides, and some heavy-fermion materials [9]. Hence, understanding how the primary exchange interaction is affected by external perturbations is essential for elucidating the origin of the macroscopic properties of many strongly coupled materials.

In this paper, we report Raman spectroscopic studies on Sr_2IrO_4 epitaxial thin films under different degrees of misfit strain induced by the substrate to reveal the interactions between the $J_{\mathrm{eff}} = 1/2$ pseudospins and the lattice. We have observed clear two-magnon peaks, which contain direct information on the exchange interactions between the $J_{\mathrm{eff}} = 1/2$ pseudospins in Sr_2IrO_4. As in-plane compressive strain is applied, the two-magnon peak is shifted to higher energies, indicating that the exchange interaction is strengthened. Moreover, the in-plane compressive strain enhances the 2D short-range magnetic order that persists at temperatures above the onset of three-dimensional long-range order. Our results thus demonstrate the substantial influence of lattice strain on the exchange interaction, which should be carefully considered to understand the physics of strongly interacting, multi-orbital systems.

Table I. Lattice parameters and misfit strain values of Sr_2IrO_4 thin films (~50 nm thick).

Samples	*a* (Å)	*c*/2 (Å)	Misfit strain tensile (+) / compressive (-)	
			In-plane (%)	Out-of-plane (%)
Sr_2IrO_4/STO	3.90	12.83	+0.4 (±0.1)	-0.50 (±0.1)
Sr_2IrO_4/LSAT	3.86	12.93	-0.7 (±0.2)	+0.32 (±0.1)

II. EXPERIMENTAL DETAILS

The Sr_2IrO_4 epitaxial thin-films were grown by pulsed laser deposition (PLD) on various oxide single-crystal substrates, *i.e.* $SrTiO_3$ (001) (STO), $(LaAlO_3)_{0.3}(Sr_2TaAlO_6)_{0.7}$ (001) (LSAT), $NdGaO_3$ (110) (NGO), and $LaAlO_3$ (110) (LAO), with the orientations of the *c*-axis perpendicular to the substrate surface. We have selected these substrates because their in-plane lattice mismatches ($\equiv \frac{a_{substrate}-a_{bulk}}{a_{substrate}} \times 100\ \%$) with bulk single-crystal Sr_2IrO_4 provide a wide range of values, *i.e.* +0.4 % (STO), -0.5 % (LSAT), -2.0 % (NGO), and -2.6 % (LAO), thereby covering both tensile (positive sign) and compressive (negative sign) strain. The thickness of the Sr_2IrO_4 thin films is kept at ~50 nm, to obtain enough Raman cross-section from the thin films while avoiding major relaxation of the misfit strain. The details of the PLD conditions are described in Refs. [10,11]. From X-ray diffraction reciprocal space mapping (Fig. 1 (a) and Fig. S1), the volume-averaged strain values ($\equiv \frac{a_{film}-a_{bulk}}{a_{bulk}} \times 100\ \%$) are estimated about +0.4 % (STO), -0.7 % (LSAT), -1.9 % (NGO), and -1.2 % (LAO), as summarized in Table I. The thin films grown on NGO and LAO substrates exhibit incoherent lattice strain relaxation (Fig. S1) presumably due to relatively large in-plane lattice mismatches between the films and the substrates. Hence, here we focus on the Sr_2IrO_4 thin films grown on STO and LSAT substrates. Since the thermal expansion coefficients of these oxide substrates are known to be similar (~10^{-5} K^{-1}) [12], we assume that the lattice strain is essentially maintained at low temperatures. Compared to the hydrostatic pressure-dependent study of Sr_2IrO_4 single crystals [13], note that the epitaxial strain here is less than about 2 GPa in pressure. Hence, it is a good tuning parameter for studying the interactions between the $J_{eff} = 1/2$ pseudospins since the intermixing of the $J_{eff} = 1/2$ and 3/2 states is expected at much higher pressure.

The Raman spectra of the Sr_2IrO_4 thin films were obtained by using a confocal micro-Raman (JobinYvon LabRam HR800) spectrometer with a focused beam spot size of ~5 μm, as shown schematically in Fig. S2 (a), with the 632.8 nm (1.96 eV) excitation line of a HeNe laser and a 600 grooves/mm grating with energy resolution ~5 cm^{-1}. Note that the photon energy of the laser, 1.96 eV, is near the charge-transfer gap (from O $2p$ to Ir $5d$ bands) of Sr_2IrO_4 [14], thereby resulting in effective resonant Raman scattering. The power of the laser at the sample surface is kept below ~0.8 mW to minimize laser heating effects. The temperature at the sample was confirmed by measuring the intensity ratio of low-energy phonon modes of the substrates in Stokes and Anti-Stokes regimes. Since the mass of the substrates is about 10^4 times larger than those of the thin films and the optical gap energies of the substrates (> 3 eV) are much higher than the 1.96 eV excitation energy, it is reasonable to assume that the thin films are in thermal equilibrium with the substrates at each temperature. The Raman spectra of the thin films are extracted by subtracting the substrates' contributions from the raw spectra measured with an optimally focused beam and the confocal setup shown in Fig. S2 (b), as described in Refs. [15,16]. Figure S2 (c) shows that the A_{1g}+B_{1g}, B_{2g}, A_{1g}+B_{2g}, and B_{1g} phonon modes are observed in the polarization-dependent backscattering channels $z(xx)\bar{z}$, $z(xy)\bar{z}$, $z(x'x')\bar{z}$, and $z(x'y')\bar{z}$, respectively, where the axes x' and y' are along the Ir-O bond direction and the axes x and y are rotated 45° from the bond [17]. These polarization-dependent phonon selection rules are consistent with those of Sr_2IrO_4 single crystals, as reported in Ref. [18].

We checked if there is any evidence of oxygen vacancies, of which precise control is a formidable task in the synthesis of complex oxide thin films. It is known that a new phonon mode at ~258 cm^{-1} (32 meV) in $z(xx)\bar{z}$ polarization emerges in oxygen-deficient Sr_2IrO_4 [19].

However, this oxygen-vacancy mode (V_O) is absent in the Raman spectra of our thin-film samples, as shown in Fig. 1 (b), indicating that the density of oxygen vacancies in our Sr_2IrO_4 thin films remains negligible owing to the relatively high oxygen partial pressure (P_{O_2} = 10 mTorr) used during the thin-film synthesis and post-annealing procedures.

III. EXPERIMENTAL RESULTS

We have observed broad B_{2g} peaks originating from two-magnon scattering at ~1320 cm^{-1} in all of the Sr_2IrO_4 thin films at low temperatures, as shown in Fig. 2 (a) and Fig. S3 (a). As the temperature increases, the spectral weight of the two-magnon peak weakens due to magnon-magnon interactions. The overall spectral shape of the two-magnon scattering is consistent with that observed in Sr_2IrO_4 single crystals [18,20]. Note that such a clear two-magnon peak is not always seen in Sr_2IrO_4 bulk crystals, particularly in off-stoichiometric samples, as discussed in Refs. [21,22]. Hence, our results confirm that these Sr_2IrO_4 thin film samples are free from extensive off-stoichiometry, regardless of the misfit strain. The two-magnon peak energy allows us to directly estimate the exchange interaction (J) of the $J_{\mathrm{eff}} = 1/2$ pseudospins in the Sr_2IrO_4 thin films. According to the two-dimensional (2D) Heisenberg model utilizing $S = 1/2$ with quantum fluctuations, the two-magnon peak energy is expected to be approximately at $2.7J$ [23], which is reduced from the classical prediction of $3J$ [24]. Since the nearest-neighbor J of Sr_2IrO_4 is known to be ~60 meV [25], the observed two-magnon peak at ~1320 cm^{-1} (~164 meV, implying $J \approx 60$ meV) is very reasonable, as also discussed for Sr_2IrO_4 single crystals in Ref. [18]. However, the asymmetric shape of the two-magnon scattering is not quantitatively understood, preventing fitting to concrete model calculations at this moment. There are some ideas including a recent theoretical work [26] suggesting that the asymmetric shape might arise from amplitude fluctuations of the magnetic order parameter, the so-called Higgs mode.

Alternatively, longer-range exchange interactions may also affect the shape of the two-magnon feature [19]. Regardless of details of the line shape, we have determined the two-magnon peak energies ($\omega_{2\mathrm{M}}$) through fits to a model function comprising two Lorentz oscillators, with imaginary part $\chi"(\omega) = \chi"_1(\omega) + \chi"_2(\omega) = \sum_{n=1}^{2} \frac{a_n \cdot \Gamma_n \cdot \omega_{2\mathrm{M}_n} \cdot \omega}{({\omega_{2\mathrm{M}_n}}^2 - \omega^2)^2 + \Gamma_n^2 \cdot \omega^2}$, where a_n and Γ_n are the amplitude and the width of the n-th mode, respectively. This phenomenological function fits the experimental spectra very well, as shown in Fig. 2 (b).

Note that the two-magnon peaks (ω_{2M_1}) shift to higher energies as compressive strain is applied to the Sr_2IrO_4 thin films. To confirm the two-magnon Raman scattering peak shift, we have calculated the integrated intensities of the raw spectra, *i.e.* the spectral weights, as a function of Raman shift. The result also shows clear blueshift (Fig. S4). Hence, the observation of the two-magnon peak shift does not depend on details of the curve fitting, but should be regarded as a robust experimental result. Figure 3 (a) summarizes the two-magnon peak energies (ω_{2M_1}) as a function of temperature. The shift of the peak maximum from Sr_2IrO_4/STO (+0.4 % tensile strain) to Sr_2IrO_4/LSAT (-0.7 % compressive strain) is approximately 50 cm^{-1} (6.2 meV) at 10 K. At higher temperatures than 10 K, a similar increase of $\omega_{2\mathrm{M}}$ values is also observed in Sr_2IrO_4/LSAT compared to Sr_2IrO_4/STO, until the two-magnon peak becomes very broad near T_N, as indicated in the increase of Γ_1 upon heating (Fig. 3 (b)). This experimental observation indicates that the overall 1 % change of the in-plane compressive strain enhances J by about 4 % ($\Delta J \approx 2.2$ meV), *i.e.* from $J = 61.1$ meV (Sr_2IrO_4/STO) to $J = 63.2$ meV (Sr_2IrO_4/LSAT). From *dc*-magnetometry measurements using a superconducting quantum interference device, we have observed that the Néel temperature (T_N) also increases about 4 % (~10 K) due to the increased compressive strain from Sr_2IrO_4/STO to Sr_2IrO_4/LSAT, as shown in the inset of Fig. 3 (b) [27].

The increased T_N is consistent with the increased J since both parameters should be monotonically related in antiferromagnetic systems.

It is tempting to explain these observations with a simple magneto-striction effect. However, the increase of J with compressive strain contradicts the widely held picture that metal oxides with perovskite structure respond to strain primarily via tilts and rotations of rigid metal-oxide octahedra, as in the Glazer description [28]. The hopping integral (t) is proportional to $\frac{\sin\theta/2}{d_{\mathrm{Ir-O}}^{3.5}}$, where θ is the bond angle of Ir-O-Ir and $d_{\mathrm{Ir\text{-}O}}$ is the bond length between Ir and O ions in the IrO_2 planes. The modest misfit strain of less than a few percents is expected to reduce θ rather than $d_{\mathrm{Ir\text{-}O}}$ according to the rigid octahedral picture. Hence, compressive misfit strain should not increase but decrease t and J since $J \propto \frac{t^2}{\widetilde{U}}$, where $\widetilde{U}$ is the effective on-site Coulomb interaction. However, our experimental data clearly demonstrate the opposite scenario, *i.e.* J increases as compressive strain is applied to Sr_2IrO_4 thin films.

IV. COMPUTATIONAL RESULTS

To understand our observations, we have performed *ab initio* calculations and found that the effective Heisenberg interaction of the $J_{\mathrm{eff}} = 1/2$ pseudospins increases as the in-plane compressive strain increases. We have employed the Vienna *ab initio* simulation package (VASP) code to relax the ionic positions of Sr_2IrO_4 under the constraint of different in-plane lattice strains. The details of the nearest and second nearest-neighbor hopping parameters of the t_{2g} orbitals using the optimized lattice constants and θ are described in the Supplemental Material [17] (see, also, references [29-36] therein). As expected, the hopping integral between d_{xy}-orbitals (t_{xy}) slightly decreases under compressive strain due to the decrease of θ. However, the compressive strain enhances the d_{xz} (d_{yz}) hopping integral, t_{xz} (t_{yz}), along the x (y)-axis.

Therefore, the overall hopping integral $t = \frac{1}{\sqrt{3}}\left(t_{xy} + t_{yz} + t_{xz}\right)$ of the $J_{\mathrm{eff}} = 1/2$ pseudospins increases under compressive strain. Furthermore, due to the staggered rotation of the IrO_6 octahedra, the inter-orbital hopping $t_z = \frac{1}{\sqrt{2}}\left(t_{xz,yz} - t_{yz,xz}\right)$ [7], where $t_{xz,yz}$ and $t_{yz,xz}$ are the off-diagonal terms in the t_{2g} matrix, also increases under the compressive strain. Projecting the t_{2g} orbitals onto the $J_{\mathrm{eff}} = 1/2$ manifold and taking the large Hubbard U limit leads to an antiferromagnetic Heisenberg model with $J = \sqrt{J_1^2 + D^2}$, where $J_1 = 4\frac{t^2 - t_z^2}{U}$ and D represents the Dzyaloshinskii-Moriya (DM) interaction proportional to $\frac{8tt_z}{U}$ [7]. The effective SU(2) Heisenberg model is obtained because t_z can be absorbed into t by a unitary transformation [4]. The results are summarized in Table II where $\widetilde{U} = U - J_{\mathrm{H}} = 2$ eV and J_{H} is the Hund's coupling. Note that both J_1 and D increase because the effective hopping integrals of the $J_{\mathrm{eff}} = 1/2$ pseudospins originate from a mixture of t_{2g} orbitals and θ has opposite effects on the t_{2g} orbitals. The second-nearest neighbor Heisenberg interaction (J_2) is of the order of 1 meV, so we ignored its contribution to the magnon energy [37]. The calculations show qualitatively consistent results with our experiments.

Table II. Effective hopping parameters t and t_z, Heisenberg, and DM interactions for $J_{\mathrm{eff}} = 1/2$ pseudospin obtained for various in-plane lattice strain.

	Pseudo-cubic in-plane (Å)	t (meV)	t_z (meV)	J (meV)	J_1 (meV)	$\lvert D\rvert$ (meV)
Sr_2IrO_4/STO	3.90	157	19	50	49	12
Sr_2IrO_4/LSAT	3.87	159	17	51	50	11
Sr_2IrO_4/LAO	3.79	171	20	60	58	14

V. DISCUSSION

The increased t under compressive strain also answers a puzzling observation of an optical spectroscopic study, namely the shift of the optical gap of magnitude ~0.3 eV to lower energies under compressive strain [10]. Since the low-energy optical absorption is understood as an optical transition from the lower Hubbard band to the upper Hubbard band of the $J_{\mathrm{eff}} = 1/2$ state, *i.e.* the Mott-Hubbard gap, its energy is proportional to U/t [14,38]. This observation has been debated because the compressive strain is expected to decrease θ and t, as generally believed in the rigid octahedral picture of transition metal oxides. However, if compressive strain enhances t due to the multi-orbital character of the $J_{\mathrm{eff}} = 1/2$ pseudospins in this layered iridate, the red-shift of the Mott-Hubbard gap can thus be understood consistently with the reduced U/t and the increased two-magnon peak energy observed in this study.

It is also noteworthy that the spectral intensities of the two-magnon peaks at $T > T_N$ for the samples under compressive strain, *i.e.* Sr_2IrO_4/LSAT, Sr_2IrO_4/NGO, and Sr_2IrO_4/LAO, are remarkably higher than the tensile-strained Sr_2IrO_4/STO due to enhanced short-range magnetic order in this quasi-2D system. The two-magnon density of states is dominated by zone-boundary excitations, which can be approximated as local spin flips, reflecting quasi-2D spin-spin correlations. Hence, the two-magnon peak intensities are often observed at temperatures above the onset of long-range magnetic order, *i.e.* above T_N, as known for La_2CuO_4 [39]. Indeed, Figure 2 (a) shows that the two-magnon peaks have non-zero intensities at temperatures above T_N. The integrated two-magnon intensities from 900 cm^{-1} to 2500 cm^{-1} are plotted as a function of temperature in Fig. 3 (c). Whereas Sr_2IrO_4/STO with tensile strain shows little two-magnon scattering intensity at room temperature (300 K), Sr_2IrO_4/LSAT with compressive strain exhibits clear non-zero two-magnon peak intensities even at 320 K, which is about 80 K higher than T_N.

It is interesting to consider why the difference of T_N between Sr_2IrO_4/LSAT and Sr_2IrO_4/STO is only about 10 K whereas the short-range magnetic order, observed by the two-magnon peak intensities, survives at much higher temperatures for the compressively strained sample. In this quasi-2D antiferromagnetic system, long-range magnetic ordering is governed by small but non-negligible interlayer interactions, which cannot be measured by our current approach. However, it is reasonable to assume that the interlayer interactions are inversely proportional to the interlayer distance, which can be modified by in-plane strain in the hypothesis of elastic deformation. As summarized in Table I, the tensile strain in Sr_2IrO_4/STO reduces the *c*-axis lattice parameter of the Sr_2IrO_4 thin film while the compressive strain in Sr_2IrO_4/LSAT causes relatively small elongation along the *c*-axis. This is presumably because the thermodynamically stable phase of Sr_2IrO_4 has somewhat elongated IrO_6 octahedra with a tetragonal distortion, preventing a further increase in the *c*-axis lattice parameters. The effect of in-plane tensile strain, which reduces J within the quasi-2D layers, on T_N may thus be partially compensated by an enhanced interlayer coupling, thus reducing the overall effect.

Finally, we discuss possible extrinsic factors such as defects other than lattice strain that can affect the experimental observations above. One may argue that the observed change of the two-magnon peak as a function of misfit strain might be caused by different oxygen stoichiometry in these thin-film samples. However, as discussed earlier, the oxygen-vacancy mode at ~258 cm^{-1} (32 meV) [19] is not observed in the Raman spectra of $z(xx)\bar{z}$ polarization (Fig. 1 (b)). Hence, it is reasonable to assume that the density of oxygen vacancies is negligible in our Sr_2IrO_4 thin films. Therefore, we exclude oxygen deficiencies as a primary reason for the changes in the two-magnon peaks in these Sr_2IrO_4 thin films.

VI. CONCLUSION

Our Raman spectroscopic studies show that the magnitude of J and the short-range magnetic order of the $J_{\mathrm{eff}} = 1/2$ pseudo-spins in Sr_2IrO_4 can be modified by lattice strain. Our observations seem somewhat counterintuitive at first glance: whereas small compressive strain (less than a few percents) is considered to decrease the metal-oxygen-metal bond angles and t between neighboring sites in many transition metal oxides, our experimental and theoretical results on Sr_2IrO_4 thin films demonstrate that compressive strain enhances J and t between the Ir sites. We find that this unexpected behavior is related to the multi-orbital characteristics of the $J_{\mathrm{eff}} = 1/2$ wave functions in this layered iridate, which is distinct from orbitally non-degenerate $S = 1/2$ systems of other transition-metal oxides. Hence, when the $J_{\mathrm{eff}} = 1/2$ pseudospin is mapped into $S = 1/2$, its multi-orbital nature and coupling with lattice should be considered carefully. Detailed analysis of temperature-dependent phonon modes using high-resolution Raman spectroscopy will also be useful to clarify this issue. However, extracting thin-film phonon spectra is difficult because the raw spectra contain significant contributions of sharp modes from the substrate at low temperatures, and is therefore left for future work.

Our results also suggest some interesting questions and perspectives. For example, to what extent will the lattice strain be effective in enhancing the exchange interaction of the pseudospins? In other words, is it possible to quench the orbital dynamics by large strain so that new electronic and magnetic ground states could emerge via strong spin-orbit coupling? Our current approach of epitaxial growth of thin films is rather limited for this purpose since strain relaxation is expected for higher lattice mismatch. However, the combination of Raman and X-ray spectroscopies with external hydrostatic or uniaxial pressure in future studies could shed further light on the coupling between the lattice and pseudospins of layered iridates.

Acknowledgment

We thank J. Yu, G. Khaliullin, J. Kim, B. J. Kim, and E. M. Pärschke for fruitful discussions. The sample synthesis and characterizations were supported by National Science Foundation Grant No. DMR-1454200. A.S. acknowledges the support (Research Fellowship for Experienced Researchers) from the Alexander von Humboldt Foundation. B.K. acknowledges financial support from the Deutsche Forschungsgemeinschaft (DFG, German Research Foundation) – Projektnummer 107745057 - TRR 80. The theoretical work was supported by the Natural Sciences and Engineering Research Council of Canada and the Center for Quantum Materials at the University of Toronto (P.P.S., H.Y.K.). The computations were performed on the GPC and Niagara supercomputers at the SciNet HPC Consortium. SciNet is funded by the Canada Foundation for Innovation under the auspices of Compute Canada; the Government of Ontario; Ontario Research Fund - Research Excellence; and the University of Toronto.

Figure Captions

FIG. 1. (a) X-ray reciprocal space maps around the pseudo-cubic 103-reflection of STO and LSAT substrates. $Q_{//} \equiv 2\pi/a$ and $Q_{\square} \equiv 2\pi/c$, where a and c are in-plane and out-of-plane lattice parameters, respectively. The $11\underline{18}$-reflections from the Sr_2IrO_4 thin films are visible. The average lattice parameters of the Sr_2IrO_4 thin films are obtained and listed in Table I. **(b)** Raman spectra of Sr_2IrO_4/STO, Sr_2IrO_4/LSAT, and Sr_2IrO_4/LAO taken at 10 K using the $z(xx)\bar{z}$ channel (A_{1g} and B_{1g}). Oxygen deficient Sr_2IrO_4 is known to exhibit an oxygen-vacancy-related mode (V_O) at the Raman shift indicated by the dotted line (~258 cm^{-1}) [19], which is not observed in these spectra. The peaks at ~278 cm^{-1} are an A_{1g} phonon mode of Sr_2IrO_4 [20].

FIG. 2. (a) Temperature-dependent Raman spectra of B_{2g} modes for Sr_2IrO_4/STO and Sr_2IrO_4/LSAT. The black triangles (▼) indicate the two-magnon peak energies at the lowest temperature (10 K). Sharp peaks at lower energies (< 800 cm^{-1}) are B_{2g} phonons. **(b)** Raman spectra of B_{2g} modes for Sr_2IrO_4/STO and Sr_2IrO_4/LSAT at 10 K. The solid lines are curve fits using two Lorentz oscillators for the broad, asymmetric two-magnon peaks above 900 cm^{-1}. The obtained two-magnon peak positions show a blueshift of ~50 cm^{-1} from Sr_2IrO_4/STO to Sr_2IrO_4/LSAT.

FIG. 3. (a) The two-magnon peak energies of Sr_2IrO_4/STO and Sr_2IrO_4/LSAT as a function of temperature. **(b)** The two-magnon peak widths of Sr_2IrO_4/STO and Sr_2IrO_4/LSAT as a function of temperature. The inset shows magnetizations vs. temperature measured with field-cooling at H = 100 Oe for the Sr_2IrO_4/STO and Sr_2IrO_4/LSAT samples. **(c)** The normalized spectral weights, *i.e.* the integrated intensities from 900 cm^{-1} to 2500 cm^{-1}, of the two-magnon peaks as a function of temperature. The vertical dashed lines of blue and red color indicate T_N of Sr_2IrO_4/STO and Sr_2IrO_4/LSAT samples, respectively, obtained from the inset of Fig. 3 (b).

References

[1] W. Witczak-Krempa, G. Chen, Y. B. Kim, and L. Balents, Annu. Rev. Condens. Matter Phys. **5**, 57 (2014).

[2] B. J. Kim, H. Jin, S. J. Moon, J. Y. Kim, B. G. Park, C. S. Leem, J. Yu, T. W. Noh, C. Kim, S. J. Oh, J. H. Park, V. Durairaj, G. Cao, and E. Rotenberg, Phys. Rev. Lett. **101**, 076402 (2008).

[3] R. Comin, G. Levy, B. Ludbrook, Z. H. Zhu, C. N. Veenstra, J. A. Rosen, Y. Singh, P. Gegenwart, D. Stricker, J. N. Hancock, D. van der Marel, I. S. Elfimov, and A. Damascelli, Phys. Rev. Lett. **109**, 266406 (2012).

[4] F. Wang and T. Senthil, Phys. Rev. Lett. **106**, 136402 (2011).

[5] H. Watanabe, T. Shirakawa, and S. Yunoki, Phys. Rev. Lett. **110**, 027002 (2013).

[6] Y. K. Kim, O. Krupin, J. D. Denlinger, A. Bostwick, E. Rotenberg, Q. Zhao, J. F. Mitchell, J. W. Allen, and B. J. Kim, Science **345**, 187 (2014).

[7] J.-M. Carter, V. Shankar V., and H.-Y. Kee, Phys. Rev. B **88**, 035111 (2013).

[8] G. Jackeli and G. Khaliullin, Phys. Rev. Lett. **102**, 017205 (2009).

[9] D. J. Scalapino, Rev. Mod. Phys. **84**, 1fsh383 (2012).

[10] J. Nichols, J. Terzic, E. G. Bittle, O. B. Korneta, L. E. D. Long, J. W. Brill, G. Cao, and S. S. A. Seo, Appl. Phys. Lett. **102**, 141908 (2013).

[11] S. S. A. Seo, J. Nichols, J. Hwang, J. Terzic, J. H. Gruenewald, M. Souri, J. Thompson, J. G. Connell, and G. Cao, Appl. Phys. Lett. **109**, 201901 (2016).

[12] A. Okazaki and M. Kawaminami, Mater. Res. Bull. **8**, 545 (1973).

[13] D. Haskel, G. Fabbris, M. Zhernenkov, P. P. Kong, C. Q. Jin, G. Cao, and M. van Veenendaal, Phys. Rev. Lett. **109**, 027204 (2012).

[14] C. H. Sohn, M.-C. Lee, H. J. Park, K. J. Noh, H. K. Yoo, S. J. Moon, K. W. Kim, T. F. Qi, G. Cao, D.-Y. Cho, and T. W. Noh, Phys. Rev. B **90**, 041105 (2014).

[15] M. Hepting, M. Minola, A. Frano, G. Cristiani, G. Logvenov, E. Schierle, M. Wu, M. Bluschke, E. Weschke, H. U. Habermeier, E. Benckiser, M. Le Tacon, and B. Keimer, Phys. Rev. Lett. **113**, 227206 (2014).

[16] M. Hepting, D. Kukuruznyak, E. Benckiser, M. Le Tacon, and B. Keimer, Physica B **460**, 196 (2015).

[17] See Supplemental Material at http://link.aps.org/supplemental/... for further experimental and computational details.

[18] H. Gretarsson, N. H. Sung, M. Höppner, B. J. Kim, B. Keimer, and M. Le Tacon, Phys. Rev. Lett. **116**, 136401 (2016).

[19] N. H. Sung, H. Gretarsson, D. Proepper, J. Porras, M. Le Tacon, A. V. Boris, B. Keimer, and B. J. Kim, Philos. Mag. **96**, 413 (2016).

[20] H. Gretarsson, J. Sauceda, N. H. Sung, M. Höppner, M. Minola, B. J. Kim, B. Keimer, and M. Le Tacon, Phys. Rev. B **96**, 115138 (2017).

[21] J.-A. Yang, Y.-P. Huang, M. Hermele, T. Qi, G. Cao, and D. Reznik, Phys. Rev. B **91**, 195140 (2015).

[22] M. F. Cetin, P. Lemmens, V. Gnezdilov, D. Wulferding, D. Menzel, T. Takayama, K. Ohashi, and H. Takagi, Phys. Rev. B **85**, 195148 (2012).

[23] W. H. Weber and G. W. Ford, Phys. Rev. B **40**, 6890 (1989).

[24] P. A. Fleury and R. Loudon, Phys. Rev. **166**, 514 (1968).

[25] J. Kim, D. Casa, M. H. Upton, T. Gog, Y.-J. Kim, J. F. Mitchell, M. van Veenendaal, M. Daghofer, J. van den Brink, G. Khaliullin, and B. J. Kim, Phys. Rev. Lett. **108**, 177003 (2012).

[26] S. A. Weidinger and W. Zwerger, Eur. Phys. J. B **88**, 237 (2015).

[27] Due to the large paramagnetic moments of Nd *f*-electrons and magnetic impurities, we could not obtain the magnetization data from Sr_2IrO_4/NGO and Sr_2IrO_4/LAO samples.

[28] A. M. Glazer, Acta Crystallogr. B **28**, 3384 (1972).

[29] G. Kresse and J. Furthmüller, Phys. Rev. B **54**, 11169 (1996).

[30] G. Kresse and D. Joubert, Phys. Rev. B **59**, 1758 (1999).

[31] J. P. Perdew, A. Ruzsinszky, G. I. Csonka, O. A. Vydrov, G. E. Scuseria, L. A. Constantin, X. Zhou, and K. Burke, Phys. Rev. Lett. **100**, 136406 (2008).

[32] J. P. Perdew, A. Ruzsinszky, G. I. Csonka, O. A. Vydrov, G. E. Scuseria, L. A. Constantin, X. Zhou, and K. Burke, Phys. Rev. Lett. **102**, 039902 (2009).

[33] S. L. Dudarev, G. A. Botton, S. Y. Savrasov, C. J. Humphreys, and A. P. Sutton, Phys. Rev. B **57**, 1505 (1998).

[34] N. Marzari and D. Vanderbilt, Phys. Rev. B **56**, 12847 (1997).

[35] I. Souza, N. Marzari, and D. Vanderbilt, Phys. Rev. B **65**, 035109 (2001).

[36] A. A. Mostofi, J. R. Yates, Y.-S. Lee, I. Souza, D. Vanderbilt, and N. Marzari, Comput. Phys. Commun. **178**, 685 (2008).

[37] From the resonant inelastic X-ray scattering experiment of Ref. [25], the second-nearest (J_2 = -20 meV) and third-nearest (J_3 = 15 meV) neighbor couplings are estimated an order of magnitude larger than the values of the density functional theory calculations. However, the two-magnon peak energy is determined by J_1 ($\omega_{2M} = 2.7J_1$) and the contributions from J_2 and J_3 are canceled out according to a simple broken-bond counting argument ($\omega_{2M} = 3J_1 - 4J_2 - 4J_3$). See also the Supplemental Material for details.

[38] M. Souri, B. H. Kim, J. H. Gruenewald, J. G. Connell, J. Thompson, J. Nichols, J. Terzic, B. I. Min, G. Cao, J. W. Brill, and A. Seo, Phys. Rev. B **95**, 235125 (2017).

[39] K. B. Lyons, P. A. Fleury, J. P. Remeika, A. S. Cooper, and T. J. Negran, Phys. Rev. B **37**, 2353 (1988).

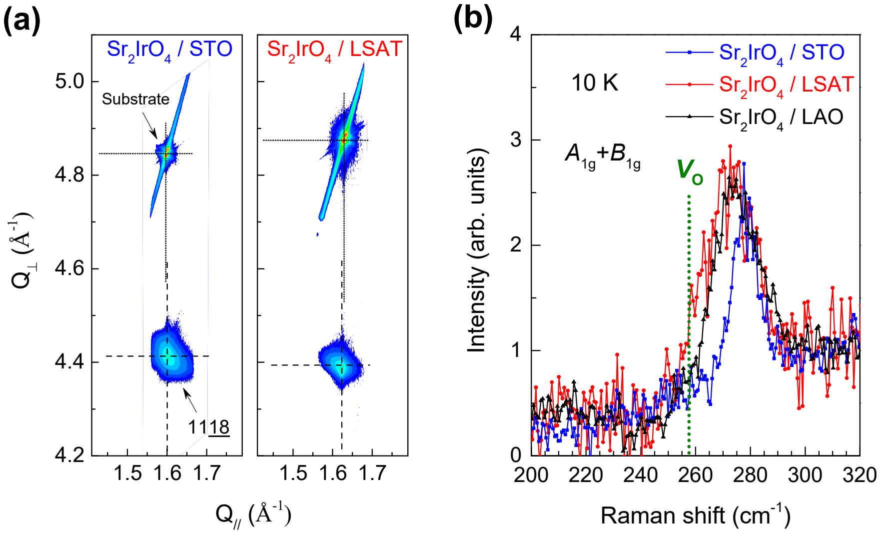

(a)
Sr2IrO4 / STO
Sr2IrO4 / LSAT
Substrate
1118
5.0
4.8
4.6
4.4
4.2
Q⊥ (Å-1)
1.5
1.6
1.7
Q// (Å-1)
(b)
10 K
A1g+B1g
VO
Sr2IrO4 / STO
Sr2IrO4 / LSAT
Sr2IrO4 / LAO
Intensity (arb. units)
0
1
2
3
4
200
220
240
260
280
300
320
Raman shift (cm-1)

Figure 1

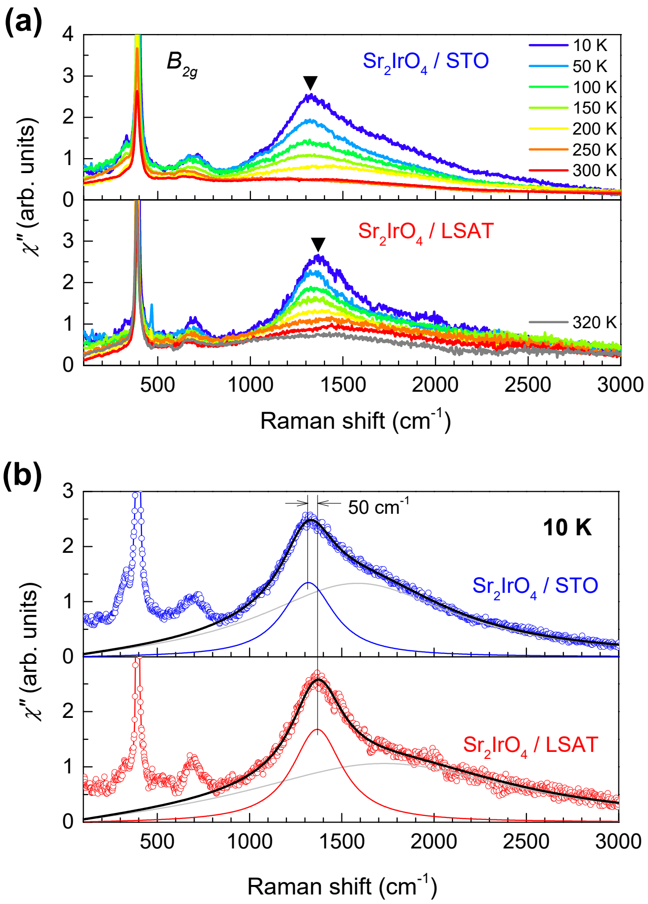
(a)
B_{2g}
Sr_2IrO_4 / STO
10 K
50 K
100 K
150 K
200 K
250 K
300 K
Sr_2IrO_4 / LSAT
320 K
χ'' (arb. units)
0
1
2
3
4
500
1000
1500
2000
2500
3000
Raman shift (cm^{-1})
(b)
50 cm^{-1}
10 K
Sr_2IrO_4 / STO
Sr_2IrO_4 / LSAT
χ'' (arb. units)
Raman shift (cm^{-1})

Figure 2

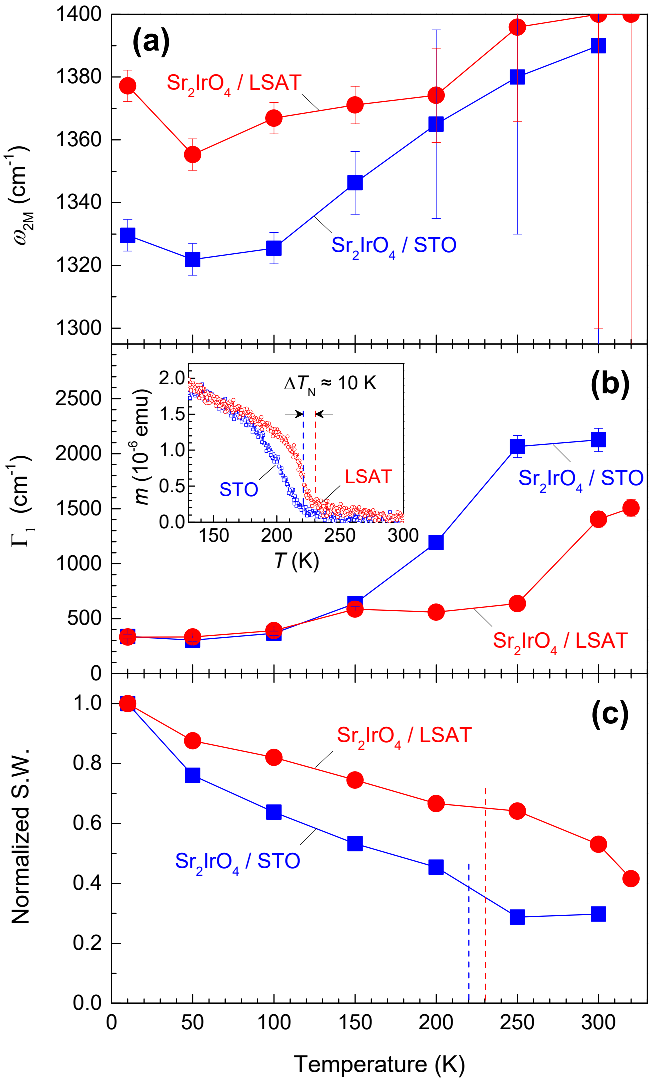
(a)
Sr$_2$IrO$_4$ / LSAT
Sr$_2$IrO$_4$ / STO
ω_{2M} (cm^{-1})
1300
1320
1340
1360
1380
1400
(b)
Γ_I (cm^{-1})
0
500
1000
1500
2000
2500
Sr$_2$IrO$_4$ / STO
Sr$_2$IrO$_4$ / LSAT
$\Delta T_N \approx 10$ K
m (10^{-6} emu)
0.0
0.5
1.0
1.5
2.0
STO
LSAT
150
200
250
300
T (K)
(c)
Normalized S.W.
0.0
0.2
0.4
0.6
0.8
1.0
Sr$_2$IrO$_4$ / LSAT
Sr$_2$IrO$_4$ / STO
0
50
100
150
200
250
300
Temperature (K)

Figure 3